Search for neutrinoless double-β decay in ^{136}Xe with a time projection chamber

J.-C. Vuilleumier, J. Busto, J. Farine, V. Jörgens, L. W. Mitchell,* M. Treichel,
and J.-L. Vuilleumier
Institut de Physique, A.-L. Breguet 1, 2000 Neuchâtel, Switzerland

H. T. Wong,† F. Boehm, P. Fisher,‡ H. E. Henrikson, D. A. Imel,§ M. Z. Iqbal,‖
B. M. O'Callaghan-Hay, and J. Thomas¶
Norman Bridge Laboratory of Physics, California Institute of Technology, Pasadena, California 91125

K. Gabathuler
Paul Scherrer Institute, 5232 Villigen-PSI, Switzerland
(Received 8 March 1993)

A xenon time projection chamber (TPC) with an active volume of 180 liters has been built to study neutrinoless double-β decay in ^{136}Xe. The experiment was performed in the Gotthard Underground Laboratory, with 5 atm of xenon enriched to 62.5% in ^{136}Xe. The experimental details, background considerations, detector performance, and data analysis are discussed. From 6830 h of data, no evidence has been found for the 0ν $0^+ \rightarrow 0^+$ transition. Half-life limits of $T^{0\nu}_{1/2} > 3.4(6.4) \times 10^{23}$ yr in the mass mechanism mode, and $T^{0\nu}_{1/2} > 2.6(4.9) \times 10^{23}$ yr in the right-handed currents mode, at the 90(68)% C.L., were derived, corresponding to an upper limit on the Majorana neutrino mass parameter $\langle m_\nu \rangle$ of about 2.8 eV. Limits on two-neutrino double-β decay of $T^{2\nu}_{1/2} > 2.1 \times 10^{20}$ yr, and on neutrinoless double-β decay with Majoron emission of $T^{0\nu\chi}_{1/2} > 4.9 \times 10^{21}$ yr, both at 90% C.L., were also derived. Accordingly, a limit on the effective Majoron-neutrino coupling parameter of $\langle g_M \rangle < 2.4 \times 10^{-4}$ was deduced.

PACS number(s): 23.40.Bw, 13.10.+q, 14.60.Gh, 27.60.+j

I. INTRODUCTION

As is well known, nuclear double-β ($\beta\beta$) decay is a process in which a nucleus (A, Z) decays spontaneously to a daughter nucleus $(A, Z+2)$ [1]. There are two principal channels for this process: neutrinoless double-β decay ($0\nu\beta\beta$),

$$(A, Z) \rightarrow (A, Z+2) + 2e^-,$$

and two-neutrino double-β decay ($2\nu\beta\beta$),

$$(A, Z) \rightarrow (A, Z+2) + 2e^- + 2\bar{\nu}_e.$$

Neutrinoless double-β decay provides a sensitive test of the standard model, as it would require violation of lepton number conservation as well as the presence of a massive Majorana neutrino. With the standard left-handed weak couplings, $0\nu\beta\beta$ are restricted to $0^+ \rightarrow 0^+$ transitions between parent and daughter nuclei [the "mass mechanism" (MM) mode]. If, in addition, there exist right-handed weak currents, the transitions thus induced can be $0^+ \rightarrow 0^+, 1^+, 2^+$ [the "right-handed-current" (RHC) mode]. The observation of $0\nu\beta\beta$ would, therefore, provide evidence of new physics beyond the standard model. It would imply (a) the neutrino is a Majorana particle and (b) there is at least one massive neutrino.

Two-neutrino double-β decay, on the other hand, is a second-order weak interaction allowed by the standard model. However, investigations in the $2\nu\beta\beta$ channel are also important, since they can reveal information on the nuclear structure, which in turn will help to interpret the measurements of the $0\nu\beta\beta$ experiments.

In order to derive information on the fundamental parameters in the neutrino sector (masses and mixing matrices) from the measured $0\nu\beta\beta$ decay rates or limits, the phase-space integrals and the nuclear matrix elements must be known. The phase-space factors depend only on the transition energies and can be calculated exactly. The nuclear matrix elements, however, are nontrivial, and their calculations are actively pursued by several groups [2].

Experimentally, $0\nu\beta\beta$ is characterized by a peak at the transition energy for the total-electron-energy spectrum, while $2\nu\beta\beta$ gives a continuous spectrum peaked at about 40% of the transition energy. The theoretical energy spectra are shown in Fig. 1. Experimental searches for double-β decay dated as early as the 1950's, but have stimulated intense interests only in the past decade [3]. There are geochemical measurements for $\beta\beta$ lifetimes in

---

*Present address: Department of Physics, Flinders University, Bedford Park, SA 5042, Australia.

†Present address: CERN PPE Division, 1211 Geneva 23, Switzerland.

‡Present address: Department of Physics and Astronomy, Johns Hopkins University, Baltimore, MD 21218.

§Present address: Jet Propulsion Laboratory, 4800 Oak Grove Drive, Pasadena, CA 91109.

‖Present address: Bellcore, 331 Newman Springs Road NVC 3X-239, Red Bank, NJ 07701.

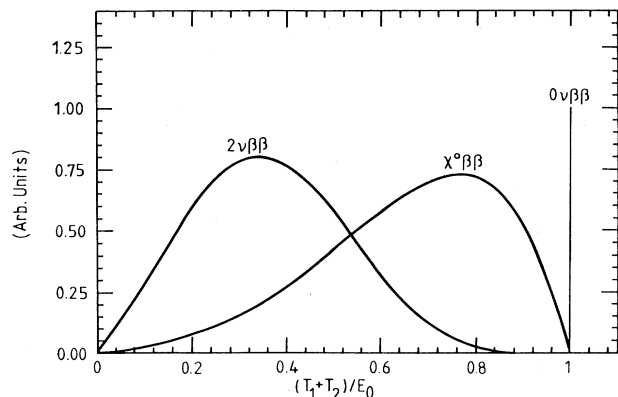¶Present address: L-397, Lawrence Livermore National Laboratory, Livermore, CA 94550.

FIG. 1. Theoretical energy spectra for the various double-β decay channels.

^{82}Se, ^{128}Te,e ^{130}Te, and ^{238}U [4], though various channels cannot be differentiated. Direct laboratory evidence for $2\nu\beta\beta$ have been obtained in ^{82}Se, ^{100}Mo, and ^{76}Ge [5]. The $0\nu\beta\beta$ channel, however, has not been observed so far. To date, the most stringent limits come from the ^{76}Ge experiments, with $T^{0\nu}_{1/2} > 1.4(2.5) \times 10^{24}$ yr at a 90(68)% C.L. [6] from a Heidelberg-Moscow group using a 86%-enriched ^{76}Ge detector.

Another more exotic channel which has received considerable interest recently is neutrinoless double-β decay with the emission of a Majoron ($0\nu\chi$):

$$(A,Z)\rightarrow(A,Z+2)+2e^- +\chi \ .$$

The Majoron is the massless Goldstone boson generated by the spontaneous breakdown of $B-L$ (baryon number minus lepton number) symmetry [7], a process that produces the Majorana mass for the neutrinos. The signature of this process is a typical three-body decay spectrum peaked at about 80% of the transition energy, as shown in Fig. 1. Recent measurements of the Irvine Time Projection Chamber (TPC) on the nuclei ^{82}Se, ^{100}Mo, and ^{150}Nd [8] indicate an intriguing excess of counts in this energy range and can be interpreted as a hint for the existence of this channel.

The isotope ^{136}Xe is an excellent candidate for double-β decay studies. Its natural abundance (8.9%) is appreciable, and xenon enriched in ^{136}Xe is commercially available [9] at a moderate price. The 0ν transition energy (2.48 MeV) is large, leading to an enhancement of the phase-space factor and decay rates, whereas the single-β decay to ^{136}Cs is kinematically forbidden. In addition, xenon is a good proportional and drift gas, and thus can act as both source and detector, enabling massive detectors to be constructed.

The possibility of conducting an experimental search for double-β decay in ^{136}Xe, with the use of a helium-xenon cloud chamber, was first investigated in 1976 [10]. Recently, experiments have been carried out by two groups: a Moscow group [11] using a high-pressure ionization chamber at the Baksan laboratory and a Milano group [12] with a multielement proportional counter at

Gran Sasso. Also notable are the efforts of a number of groups trying to develop liquid-xenon ionization chambers [13] to be applied to $\beta\beta$ experiments.

The Caltech-Neuchâtel-PSI Collaboration has been involved in experimental investigations of double-β decay at the Gotthard Underground Laboratory under the Swiss Alps. We have built a time projection chamber (TPC) [14] to study double-β decay in ^{136}Xe, in both the 0ν and 2ν channels [15]. The idea of the time projection chamber was originated by Nygren in 1975 [16]. In the Gotthard TPC, secondary electrons produced by primary ionization are drifted in a uniform electric field to the anode wires where charge multiplication occurs. Signals are electrostatically induced at a nearby XY readout plane. The time evolution of the signals gives information in the Z direction. In this way, three-dimensional track reconstruction is achieved. The energy of an event is measured by integrating the anode signals over the drift time.

The simultaneous tracking and calorimetry capabilities of the TPC make it an ideal device to study double-β decay in ^{136}Xe. A double-β decay event is identified as a continuous trajectory with the characteristic "end features" of electrons: high-charge depositions (charge "blobs") due to enhanced dE/dx at low energy and large-angle multiple scattering (that is, staggered trajectories), at *both* ends. This provides a powerful means of background suppression from α particles, cosmic rays muons, and single electrons. Using these techniques, the present experiment has already achieved more than an order of magnitude improvement in 0ν sensitivity over previous searches [11,12]. Previous results have been reported in an earlier publication [17]. We will elaborate on the experimental details in this article.

II. EXPERIMENTAL DETAILS

In order to perform a sensitive search of double-β decay in ^{136}Xe, the TPC must be able to meet the following experimental objectives: track reconstruction, dE/dx measurement (that is, blob/track differentiation), energy resolution, and low background. The detector design is, therefore, optimized for these purposes. Further details on conceptual design [18], electronics [19], and data acquisition [20] can be found in previous publications.

A. Gotthard underground laboratory

To minimize cosmic-ray-related background, the experiment is performed at the Gotthard Underground Laboratory situated in the 17-km-long St. Gotthard Road Tunnel under the Alps in Central Switzerland. The experimental hall is located in a bay (No. 59B) connecting the main road tunnel and an auxilliary emergency tunnel, approximately 4 km from the southern exit at the village of Airolo. The minimum rock overburden is 1070 m, or about 3000 meters of water, equivalent (mwe). This attenuates the muon flux by a factor 10^6 to a rate of about 10 per day at our detector. The laboratory is equipped with air conditioning and computer modem facilities.

B. Time projection chamber

The schematic diagram of the experimental setup is shown in Fig. 2. The main chamber of the TPC is a cylindrical OFHC (oxygen-free high-conductivity) copper vessel 5 cm in thickness and rated for 15 atm. The active volume is 180 liters (69.7 cm in height, 57.4 cm in diameter). The gas handling system is outside the shielding and is connected to the TPC by two right-angled fittings, to prevent direct illumination by background γ rays from outside. There are four view ports on the side for calibration purposes.

The fill gas of the TPC is xenon enriched to 62.5% of ^{136}Xe, with an admixture of 3.9% methane to increase the drift velocity and to suppress diffusion of secondary electrons [21]. The operating pressure is 5 atm, giving a total 1.46×10^{25} ^{136}Xe atoms in the active volume. According to Monte Carlo studies based on GEANT [22], the "detector containment efficiency", which is the probability for a double-β decay event at 2.5 MeV to be completely contained in the active volume of the TPC, is 30% and 27% for the MM and RHC modes, respectively. The difference is mainly due to the difference in energy distribution between the two modes [23].

The xenon-methane mixture is continuously circulated through a "hydrox" getter [24] by a magnetically driven piston pump [24]. This maintains gas purity at a level of 0.1 ppm in electronegative contaminants, and the attenuation of the drifting electrons over 70 cm is less than 2%. When not in use, the gas can be recuperated by a recovery tank cooled down to liquid-nitrogen temperature.

The cathode is at 68 kV, creating a drift field of 970 V cm^{-1}. Between the cathode and anode systems, there are equally spaced field-shaping rings connected to adjacent ones by 10-MΩ resistors to ensure field uniformity. The resulting drift velocity is 1.3 cm μs^{-1}.

The geometry and dimension of the anode system are depicted in Fig. 3. All the wires are made of gold-plated tungsten and are under uniform tension (70 g for the 20-
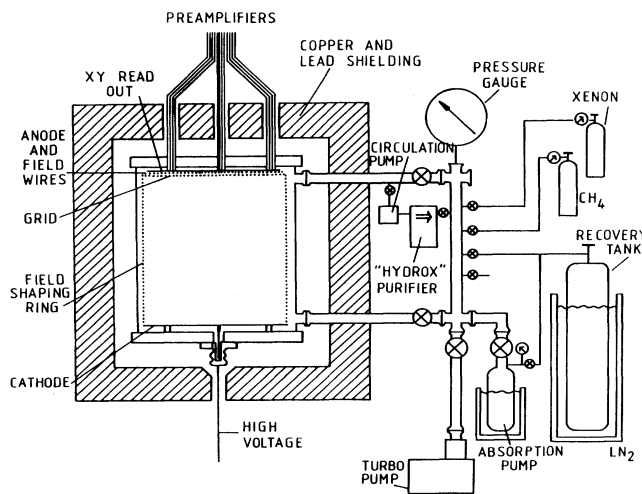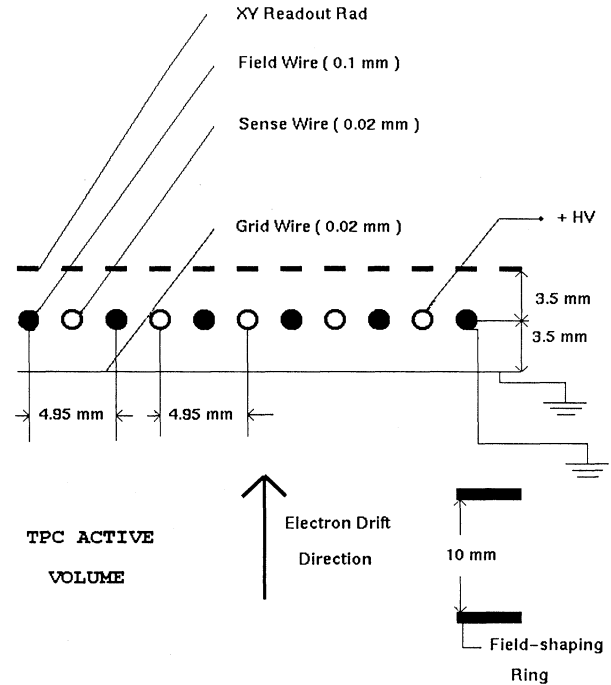
FIG. 3. TPC anode system, showing the geometrical dimension.

μm-diam anode and grid wires and 90 g for the 100-μm-diam field wires). The ends of the wires are soldered on to copper strips etched on the mounting frame. Plastic caps are placed in between the anode wires and the nearby field-wire strips, so as to avoid high-voltage discharges. The mounting frame is constructed by moulding a low-background epoxy (Araldite [25]) to a copper ring. The achieved geometrical accuracy is 25 μm. The anode voltage is about 2600 V, and the anode wires are connected together to a single current-sensitive preamplifier outside the chamber, while the field and grid wires are grounded externally.

The design of the XY readout system is shown in Fig. 4. The XY-strip pattern is etched on one side of a low-background circuit board (Rexolite 1422 [25]). An identical pattern, shifted by half a unit in both X and Y axes, is etched on the other side of the board. The holes are plated through to make the channels continuous. This pattern fills up a circle of 60 cm in diameter, corresponding
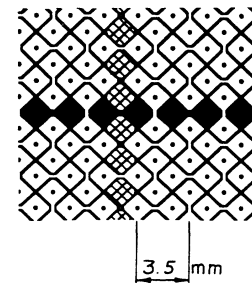
FIG. 2. Schematic diagram of the time projection chamber with the associated setup.

FIG. 4. Design of the TPC readout system for (X, Y) coordinates.

to 168 channels in each of X and Y axes with 3.5 mm pitch. Outside this pattern is the "veto ring" which defines the boundary of the measuring area. A trajectory leaving or entering the active volume of the TPC through the field-shaping ring assembly will produce signals on the veto ring, and these can be used to reject the events on line. To minimize variations of charge multiplication across the anode plane, the XY readout board is made flat by gluing it to a honeycomb structure made of Delrin [25].

C. Electronics and data acquisition

The schematic diagram of the electronics and data acquisition system is shown in Fig. 5. The TPC does not have a time-zero trigger, so that the starting time of an event is defined by the beginning of the signals from the anode wires. Data within the next 64 μs are recorded. The output of the anode preamplifier (based on the IC LeCroy TRA1000) is digitized by an 8-bit transient recorder (LeCroy TR8837F) at a rate of 8 MHz. The energy of the event is given by the integration of the transient recorder output.

Meanwhile, signals from the XY readout channels as well as the veto ring are processed by the preamplifiers and discriminators. A two-level scheme is adopted for the XY discriminators. The lower threshold above the electronic noise corresponds to *track* pixels, whereas the higher threshold indicates enhanced charge density or the *blob* pixels. The transistor-transistor logic (TTL) outputs from the discriminators are temporarily stored in the CAMAC interface modules. A trigger is generated if there is not any signal from the veto ring during the 64 μs. Following the trigger, the system waits for 4 ms to record subsequent events such as those due to delayed nuclear activity, before the CAMAC modules are read by the front-end processor (PDP 11/73).

The PDP 11/73 then compresses the data for those events that survive a simple energy cut. The data are subsequently transferred to the host computer (Tektronix 6130) via Ethernet using TCP/IP protocol. The host computer then unpacks the data and reconstructs the

events. Events which pass various on-line software routines are stored on 60-Mbyte cartridge tapes (61TC01). Various on-line diagnostic and monitoring programs are also available on the host. The data-acquisition system can typically handle about five events per second, the limiting factor to the data rate being the data compression routines in the PDP 11/73.

D. Background considerations

In low-count-rate experiments such as this one, proper understanding and control of the background is crucial. Special effort has been incorporated in the experimental design to minimize background due to cosmic rays and ambient radioactivity, as well as those from detector components, as discussed below.

1. Cosmic rays

At sea level, the rate of cosmic-ray-related events is about 100 Hz. The direct muons and hadrons can be distinguished and rejected easily, but would contribute to considerable system dead time as well as more strigent requirements for the trigger and veto systems. Even more problematic would be the background due to muon-induced events, such as muon capture by the copper vessel producing neutrons, high-energy γ rays, and radioactive isotopes. An example of this category is the ^{63}Cu$(n,\alpha+4n)^{56}$Co reaction, creating the short-lived (half-life 78.8 days) ^{56}Co which emits γ rays up to 3.3 MeV. At the Gotthard Underground Laboratory, the rate for vertical muons in the TPC is about ten per day. These events are saved for diagnostic purposes and are used to measure the drift velocity of the gas, so as to monitor the Xe-CH$_4$ ratio.

2. Natural radioactivity from surroundings

There is some level of radioactivity from the tunnel rock and laboratory equipment surrounding the TPC. The dominant sources are the ^{238}U and ^{232}Th decay chains as well as ^{40}K giving rise to γ rays up to 2.6 MeV. To minimize the background due to these events, the TPC is shielded by 20–30 cm of lead. The volume within the lead shielding is continuously purged by dry nitrogen to prevent radon gas emitted by the ^{238}U and ^{232}Th chains from diffusing in.

Another source of external background which may contribute to high-energy (>2.5 MeV) events is the thermalized neutrons produced by fission and the (α,n) reaction. Thermal neutrons captured by the nuclei are accompanied by emission of γ rays as high as 8 MeV. In particular, the reaction ^{136}Xe$(n,\gamma)^{137}$Xe results in a high-energy β decay in the active volume:

$$^{137}\text{Xe} \rightarrow {}^{137}\text{Cs} + e^- + \bar{\nu}_e$$
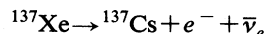
$[Q = 4.1$ MeV $(33\%)/3.6$ MeV (67%); $\tau_{1/2} = 3.9$ min$]$.

The thermal neutron flux is attenuated by the lead shielding and copper vessel by a factor of 10^3.
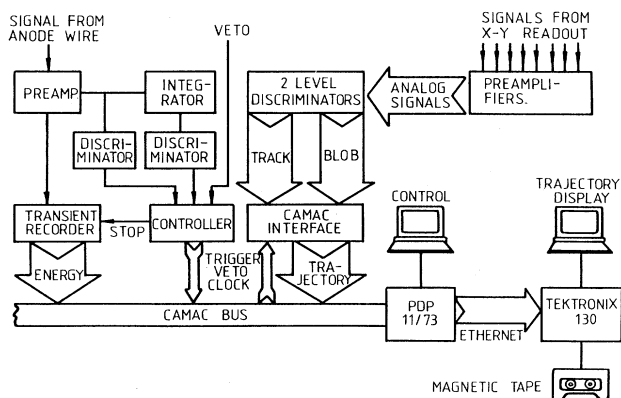

FIG. 5. Schematic diagram of the TPC electronics and data-acquisition system.

3. Natural radioactivity from internal components

Some commonly used detector components contain traces of various radioactive isotopes and have to be avoided. Accordingly, the TPC is built with low-background materials: OFHC copper for the main vessel and all metallic components, and Delrin [25] for all insulators. Other materials used inside the lead shielding constitute only a very small proportion by mass and have been tested with a low-background germanium detector, which has sensitivity in concentration of 10^{-6} for ^{40}K and 10^{-9} for both the ^{238}U and ^{232}Th chains. Materials used in the TPC, which have been tested to be radioactively clean, include rexolite and epoxy for the XY readout board, gold-plated tungsten wire, epoxy and stainless-steel pins for the anode frame, cables, and Mylar foils. However, two components (resistors and O rings) are found to contain measurable levels of radioactivity, but are currently used in the detector until suitable replacements can be found.

Although the getter materials are well outside the leading shielding, the ^{238}U and ^{232}Th chains have to be avoided since the diffusion of radon may bring radioactive isotopes into the active volume of the TPC. A measurement to look for excess of "α-particle-like" events (due to the decay of radon) shows no evidence of radon emission for the selected hydrox getter. On the contrary, circulating the gas through molecular sieve, an early candidate for getter material, produces a significant excess of α events, showing contamination of radon in the system.

Commercially available xenon contains about 15 ppm of krypton, which consists of tiny amount of ^{85}Kr (β emitter with a 687-keV end point and a 10.7-yr half-life), produced in nuclear reactors or bomb tests. While this may contribute to the low-energy background, it does not affect the sensitivity in the 0ν channel. A measurement by the Milano group [12] suggests that the amount of ^{85}Kr is considerably reduced in enriched ^{136}Xe.

III. DETECTOR PERFORMANCE

A. Track reconstruction

To illustrate the tracking capability of the TPC, some recorded events are shown in Figs. 6(a)–6(e). The XZ and YZ projections as well as the time evolution of the anode signals (sampled at 8 MHz) are displayed. There are 168 readout channels in each of X and Y axes, with a 3.5-mm pitch. A two-level scheme is adopted for the XY readout: The small dots and the large black dots indicate signals corresponding to "track" and "blob" pixels, respectively. The $Z=0$ time of the events is defined by the beginning of the anode signals. Calibration in the Z axis depends on the drift velocity of the secondary electrons. It is measured from the length of cosmic-ray muons traversing the detector vertically. Typically, a few such events are recorded per day. The Z coordinates of the trajectories are sampled at a 2-MHz rate, giving an effective bin size of 6.7 mm (at a drift velocity of 1.3 cm μs^{-1}). In the figures, the full range for both X and Y is 60 cm, while the Z calibration is 10.9 cm per unit.

A cosmic-ray-induced shower is shown in Fig. 6(a).

The display is upside down (therefore the shower cone faces up) so that the positive Z axis corresponds to the positive time axis. The following features can be observed in this event: a straight minimum ionizing muon (A), a pair production vertex (B,C), a high-energy electron which leaves the detector (D), and a low-energy electron which stops with a charge blob (E), as well as several isolated charge depositions due to photon absorption. Events such as this would be rejected on line based on the hardware veto ring.

A typical single-electron event and a typical candidate for a "two-electron" event are depicted in Figs. 6(b) and 6(c), respectively. It can be seen that the two-electron event is readily distinguishable by the features it exhibits at both ends—charge blobs and staggered trajectories. Another typical background is the multiple-site event due to interaction of high-energy γ rays, as shown in Fig. 6(d). This, again, can be identified very easily.

Figure 6(e) shows a β decay followed by the emission of an α particle at the same (X, Y) coordinate 50 μs later. This event is due to the cascade ^{214}Bi$\rightarrow$^{214}Po$+e^-+\bar{\nu}_e$ ($Q=3.28$ MeV, $T_{1/2}=19.7$ min), followed by ^{214}Po$\rightarrow$^{210}Pb$+\alpha$ ($Q=7.8$ MeV, $T_{1/2}=164$ μs), and is evidence of trace radon emission in the system. The measured rate, by selecting events with such characteristics, is 2.2 cascades per hour. The profile of the α particle is an artifact of the saturation in the electronics due to much higher charge density. Another characteristic feature for the α particles, useful in background recognition and rejection, is the large amplitude of the anode pulse compared to that of the electron track.

B. Differentiation of the "start" and "end" of tracks

The essential idea for background identification is that one can determine the directionality of electrons by studying the different characteristic features, and in particular the charge depositions, at their beginnings and ends. To investigate this quantitatively, events due to external γ sources of different energies (^{137}Cs, ^{22}Na, ^{88}Y, and ^{232}Th) are analyzed. Single-track events are selected by software, and then scanned manually to locate the coordinates of their beginnings and ends. The quantities Q_x and Q_y in the XZ and YZ projections, defined as

$$Q_x = t_x \left[1 + \left[\frac{t_x}{T} \right]^\alpha \right] + \omega b_x$$

and similarly for Q_y, are then measured. In the expression, t_x and b_x are the number of track and blob pixels in the XZ projection in a box of area $\Delta X \times \Delta Z$ centered at the located coordinate, with a relative weight of 1 to ω; T is the total number of pixels in the box; and α is an index to cast more weight to boxes where most of the pixels fire. The total charge Q associated with the coordinate is defined as the geometrical mean of the two projections:

$$Q = \sqrt{Q_x Q_y} \ .$$

The measured values of Q of the beginnings and ends are subsequently compared.

The distributions of Q for the beginnings and ends of

single-electron events are shown in Fig. 7. The chosen input parameters are $\Delta X = \Delta Y = 2.45$ cm, $\Delta Z = 3.4$ cm, $\omega = 5$, and $\alpha = 2$. The two distributions are well separated, demonstrating that (a) the ends of electron tracks can be distinguished with high efficiency from the beginnings and, hence, the directionality measured and (b) the two-

level readout scheme is sufficient to achieve this differentiation.

Above the cut of $Q = 30$, there are 1.4% of the events in the "start" distribution and 96.6% of those for the "end" distribution. Therefore the rejection efficiency for single electrons is 98.6%. It also follows that the
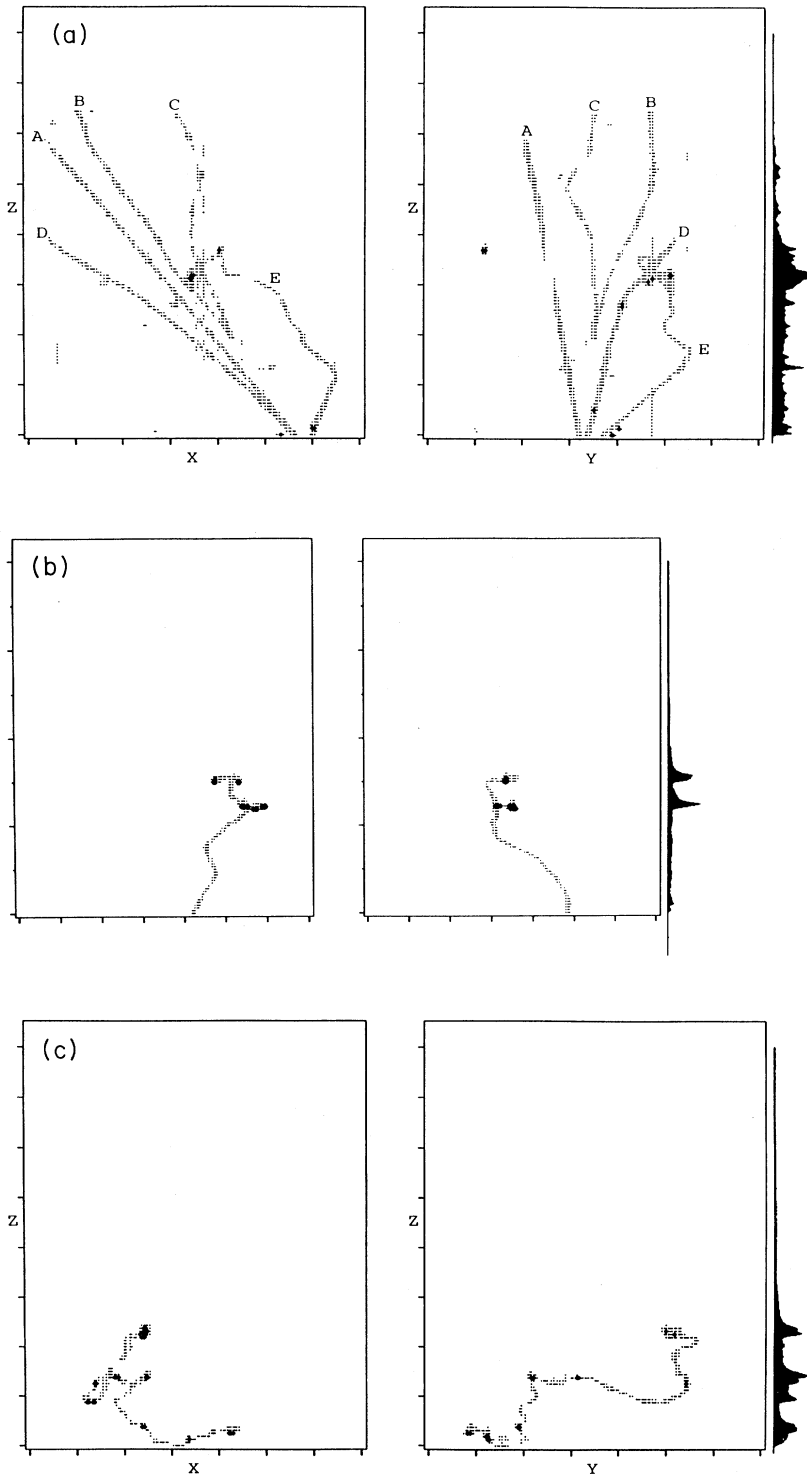

FIG. 6. Typical tracks recorded by the TPC with 5 atm of xenon: (a) cosmic-ray-induced shower, with various features ($A - E$) matched in both projections; (b) single electron; (c) two-electron candidate event; (d) multiple Compton scattering of high-energy γ rays; and (e) β decay followed by emission of an α particle. In all figures shown, the full range is 60 cm for both X and Y, while the Z calibration is 10.9 cm per unit.
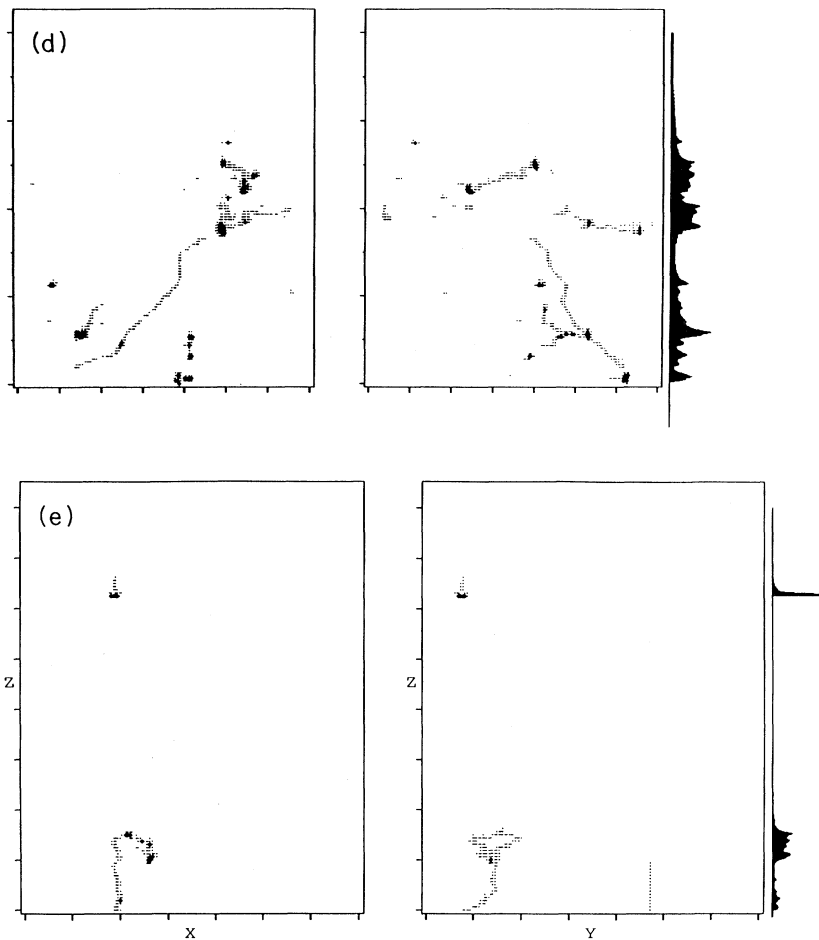
FIG. 6. (Continued).

identification of double-β events by requiring $Q > 30$ at both ends will have an efficiency of $(0.966)^2$ or 93.3%.

C. Energy resolution

The energy of an event is measured by integrating the digitized anode signals from the transient recorder over the drift time. To avoid adding up time bins with no pulses, which degrades the energy resolution, only signals with 20 mV above the dc offset are sampled. This cutoff is low compared to realistic signals so that it will not contribute to sampling error.

The energy resolution is measured with various γ sources. A 10–15 % variation in charge multiplication across the anode plane is observed. This effect is due to the limitation that the XY readout board is not absolutely flat (deviation can be up to 1 mm at the edge) so that the anode wires produce a nonuniform field gradient. To correct for this effect, the anode plane is subdivided into 45 sections and a gain variation map is made by measuring the peak positions of the ^{137}Cs 667-keV line at each section. The anode signals are then compensated in each time bin, based on the (X, Y) coordinate of the trajectory at that time. A notable improvement on the energy resolution of 14.8% and 6.6% full width at half maximum (FWHM) at 511 and 1592 keV, respectively, is subse-

quently achieved. The energy spectrum for a ^{232}Th source, after applying this gain correction, is shown in Fig. 8. The 1592-keV peak is due to double escape (pair production with the total escape of both 511-keV photons) from the incident γ rays of 2614 keV. The overall gain (combined effects of charge multiplication, gas puri-
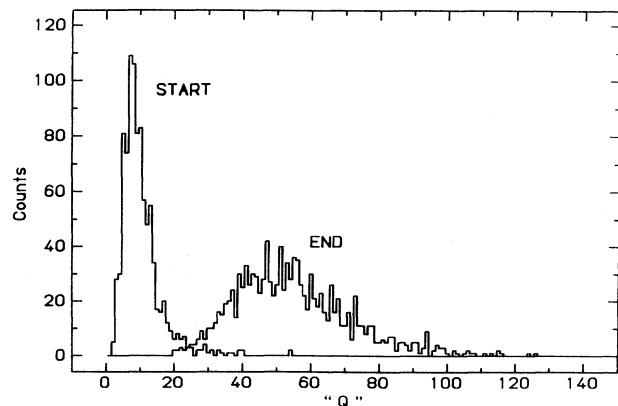

FIG. 7. Distribution of Q, as defined in Sec. III B for the "start" and "end" of electron tracks.
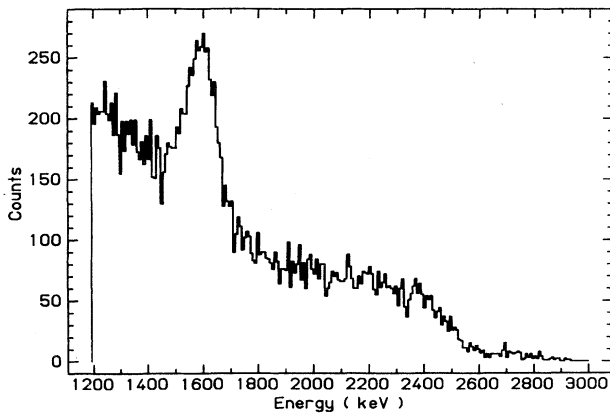
FIG. 8. Energy spectrum of a ^{232}Th source. The prominent line is the double escape peak of the 2614-keV γ rays in ^{208}Pb.

ty level, and electronics) is constant over the course of data taking to better than 2%.

Energy calibration is obtained from similar measurements on various γ spectra. It is linear in our range of interest (1–3 MeV) and is accurate to better than 2%.

IV. EVENT IDENTIFICATION

The goal of the TPC tracking is to distinguish double-β (or "two-electron") events from various possible backgroundlike α particles, cosmic-ray-related muons and showers, single electrons, and multiple Compton scattering. A double-β decay candidate event is identified by the characteristic "end features" (charge blobs and staggered trajectories) it exhibits at both ends, allowing for small isolated charge depositions (<100 keV) due to bremsstrahlung emissions. The detailed description of the various procedures for the event identification can be found in a different publication [26].

The raw trigger rates of the detector inside a shielding are about 0.9 and 0.2 Hz above 100 and 500 keV, respectively. Most of these triggers are rejected on line, either by the hardware vetos from the veto ring or by software cuts which identify the "α-like" events (from α particles and high-voltage discharges). At a typical energy threshold of 600 keV, about 40 000 events per week survive and are recorded on cartridge tape.

The off-line analysis for the $0\nu\beta\beta$ channel is subsequently performed for events above 1500 keV, using a Tektronix 4301 workstation. The major backgrounds, due to single electrons and multiple Compton scattering, are identified by a track-reconstruction program, based on their characteristic signatures: minimum ionizing (or "blobless") beginnings and multiple sites, respectively. Typically, about 84% of the initial sample is identified and rejected.

The surviving events, which amount to 350 per week, are then visually scanned. These are mostly (a) single electrons with more complex topologies which the software cannot efficiently identify, (b) tracks with blob pixels at the beginnings, and (c) events with multiple tracks which have survived the less strigent cuts. The

role of the scanner is not so much to categorize the events, but rather to assist the software analysis, particularly by matching the trajectory information in two projections into a three-dimensional (X, Y, Z) coordinate. Events with the measured Q parameter, as defined in Sec. III B greater than 30 in both ends are then categorized as "two-electron" candidate events and are put into an energy spectrum. The various cuts in these three steps are summarized in Table I. The data-reduction factor in the table denotes the fraction of events surviving a particular cut, based on a sample accepted by preceding cuts.

Of particular importance in the discussion of event identification is the inefficiency $\bar{\eta}$ of each cut, summarized also in Table I. Data taken at the same period are used in evaluating the inefficiencies. The multiplicative sum of the efficiencies $(1 - \bar{\eta}_i)$ gives the overall "analysis efficiency," which is the probability of a fully contained double-β decay event surviving all the cuts and thus being detected. The mass mechanism (MM) and right-handed-current (RHC) modes lead to different analysis efficiencies (76% and 65%, respectively) because of the difference in energy and angular distributions between the two electrons in the two modes [23]. Other major contributing factors include topological ambiguities (e.g., a track retraces itself) and detector effects (inactive or noisy electronics). As mentioned in Sec. II A, the "detector efficiencies," which are the probabilities of having a double-β event fully contained in the TPC, are 30% and

TABLE I. Data reduction and inefficiency factors for various cuts in the analysis procedures.

Cuts	Data reduction	Inefficiency ($\bar{\eta}$) MM	RHC
On-line analysis			
Hardware veto	0.5	10^{-5}	10^{-5}
Energy >600 keV	0.22	0	0
Software	0.46	$<10^{-3}$	$<10^{-3}$
Net reduction	0.051		
Off-line analysis			
Energy >1600 keV	0.06	0	0
Delayed coincidence	0.98	0	0
Events not fully contained[a]	0.93	0.0032	0.0032
"α-like" events	0.98	0.0073	0.0073
Blob count[a]	0.88		
Multiple events	0.95	0.0053	0.0053
Single electron	0.20	0.062	0.054
Net reduction	0.009		
Off-line scanning			
Energy >2000 keV	0.13	0	0
Events not fully contained[b]	0.82	0	0
Isolated charge >100 keV	0.76	0.072	0.072
One end with $Q<30$[a]	0.086		
Energy distribution		0.052	0.202
Detector response		0.067	0.067
Net reduction	0.0070		
Total reduction in data	3.2×10^{-6}		
Net analysis efficiency $=\prod_i(1-\bar{\eta}_i)$		0.76	0.65

[a]Same inefficiency factor factor, due to not having a blob at the end of the electron track.
[b]Detector efficiency not included.

27% for the MM and RHC modes, respectively. To verify these efficiency factors, double-β decay events are generated by Monte Carlo simulations and are subject to the same analysis procedures. The results are in good agreement with those derived from the actual data.

Another figure of merit for the event identification is the rejection efficiency for various categories of background. Here α particles, high-voltage discharges, cascades from decay chains, cosmic-induced showers, and muons, as well as multiple Compton scattering events (with each track more than 100 keV), can be identified with 100% efficiency since they are topologically very different from the two-electron signal. Single-electron identification is based on the difference in charge depositions between the two ends. By comparing the number of two-electron events to that of single-electron ones (identified at various stages), it can be concluded that the rejection efficiency for single electrons above 1.5 MeV is at least 98% (the value may be higher since some of the two-electron events can be due to double-β decay or pair production rather than misidentified single-electron background). This agrees well with the rejection efficiency of 98.6% derived from the "$Q=30$" cut, as discussed in Sec. III B.

V. DATA AND INTERPRETATIONS

A total of 6830 h of data, taken during the period from February 1991 to January 1992, are presented in this article. Depicted in Fig. 9 is the "two-electron" spectrum, which consists of events surviving the various cuts described in Sec. IV. There is no evidence for an excess of counts at the expected 0ν transition energy of 2.48 MeV.

As described in Sec. II C, the measured energy resolution is 6.6% at 1.6 MeV. We adopt the conservative approach of taking this to be the FWHM resolution at the 0ν energy. Based on Poisson statistics, the probability of a Gaussian peak to be present at this energy window is evaluated. Assuming an exponential background between 2000 and 2650 keV together with a constant background from 2650 to 3000 keV, we obtain an upper limit
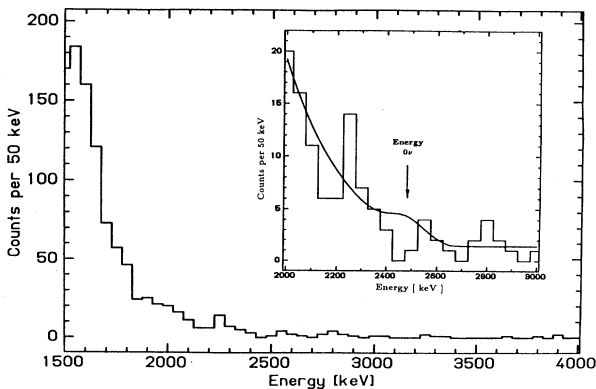
of 5.3 (2.8) events for a hypothetical 0ν peak at a 90% (68%) confidence level. The cutoff of the exponential background is chosen to be 2650 keV because the end point for natural radioactivity is at 2614 keV. It has been checked that the derived limits are not sensitive to the exact value of this cutoff.

As mentioned in Sec. II B, there are 1.46×10^{25} ^{136}Xe atoms in the fiducial volume. Folding in the detector (30% and 27%) and analysis (76% and 65%) efficiencies for the MM and RHC modes, respectively, we obtain the 90% C.L. half-life limits

$$T^{0\nu}_{1/2}(0^+ \rightarrow 0^+; \langle m_\nu \rangle) > 3.4 \times 10^{23} \text{ yr}$$

and

$$T^{0\nu}_{1/2}(0^+ \rightarrow 0^+; RHC) > 2.6 \times 10^{23} \text{ yr}.$$

The corresponding 68% C.L. limits are 6.4×10^{23} and 4.9×10^{23} yr, respectively. These limits represent a factor of 30 improvement over the other ^{136}Xe experiments [11,12] and are almost 50% better than our previous results [17]. The 90% C.L. curve is shown in the energy spectrum in Fig. 9.

The limits for the Majorana-neutrino mass parameter and the right-handed coupling parameters thus deduced depend on which nuclear matrix-element calculation [2] one adopts. To illustrate the range of sensitivities, the limits derived from the calculations of the Caltech [27], Heidelberg [28], and Tübingen [29] groups are tabulated in Table II. For comparison, the limits from the ^{76}Ge [6] and ^{128}Te [4] experiments are also shown. It can be seen that the limits on $\langle m_\nu \rangle$ from various calculations are in reasonable agreement in the case of ^{136}Xe, but vary by a factor of 2 for ^{76}Ge.

In particular, as indicated in Fig. 10(a), the Caltech calculations [27] give good agreement with the several 2ν half-lives which have been measured. Considering the range of the parameter α'_1 to be between -360 and -390 MeV fm^3, as shown in the shaded area of Fig. 10(b), we derive the 90% C.L. limit for the Majorana-neutrino mass parameter

$$\langle m_\nu \rangle < 2.8 - 4.3 \text{ eV} .$$

This is to be compared with $\langle m_\nu \rangle < 2.2 - 4.4$ eV derived from the best ^{76}Ge limit [6]. In comparison, as shown in Table II, if the geochemical lifetime measurement on ^{128}Te is interpreted to be equivalent to a $T^{0\nu}_{1/2}$ limit, the neutrino mass parameter thus deduced will be $\langle m_\nu \rangle < 1.8$ eV. However, as depicted in Fig. 10(a), the matrix-element calculations for ^{128}Te tend to have sizable uncertainties, reflected in the incorrect predictions on the 2ν lifetime with the best-fit values of α'_1 derived from the measured half-lives of ^{76}Ge, ^{82}Se, and ^{100}Mo.

Considering the theoretical uncertainties, it is essential that investigations of neutrinoless double-β decay are pursued in various nuclei, preferably with different ranges in Z. The experiment reported here is at present the only one which has achieved the $0\nu\beta\beta$ sensitivities of ^{76}Ge

FIG. 9. Energy spectrum of two-electron candidate events, from 6830 h of data. The 90% C.L. limit for a hypothetical 0ν peak at 2481 keV is represented by the solid line in the inset.

TABLE II. Limits on the neutrino mass and couplings parameters, from the Gotthard ^{136}Xe experiment and in comparison with the ^{76}Ge laboratory experiments. The limits implied by the ^{128}Te geochemical measurement are also shown.

Isotope	Mode	$T^{0\nu}_{1/2}$ (yr) (at 90% C.L.)	Parameters	Caltech	Calculations Heidelberg	Tübingen
^{136}Xe	MM	$>3.4\times10^{23}$	$\langle m_\nu\rangle$ (eV)	$<2.8-4.3$	<2.5	<2.9
	RHC	$>2.6\times10^{23}$	$|\langle\lambda\rangle|$ (10^{-6})		<4.4	<2.7
			$|\langle\eta\rangle|$ (10^{-8})		<2.3	<7.4
	Majoron	$<4.9\times10^{21}$	$\langle g_M\rangle$ (10^{-4})	<2.4	<1.7	<2.0
^{76}Ge	MM	$>1.4\times10^{24}$	$\langle m_\nu\rangle$ (eV)	$<2.2-4.4$	<1.3	<2.0
	RHC	$>1.4\times10^{24}$	$|\langle\lambda\rangle|$ (10^{-6})		<2.3	<2.4
			$|\langle\eta\rangle|$ (10^{-8})		<1.4	<5.8
	Majoron	$>3.9\times10^{22}$	$\langle g_M\rangle$ (10^{-4})	<2.8	<1.1	<1.7
^{128}Te	MM	$>7.7\times10^{24}$	$\langle m_\nu\rangle$ (eV)	<1.8	<1.0	<2.4
(Geochem.)	RHC	$>7.7\times10^{24}$	$|\langle\lambda\rangle|$ (10^{-6})		<4.2	<4.3
			$|\langle\eta\rangle|$ (10^{-8})		<1.3	<5.3
	Majoron	$>7.7\times10^{24}$	$\langle g_M\rangle$ (10^{-4})	<0.2	<0.1	<0.3

with a different isotope. The simultaneous tracking and calorimetry capabilities of the TPC, using the source as the detector medium, prove to be ideal for double-β decay investigations.

In addition, this experiment has achieved a remarkably low-background level after event identification, owing to the powerful tracking capabilities of the TPC. The measured background rate of 0.01 counts keV^{-1} kg^{-1} yr^{-1} at the 0ν energy range represents an order of magnitude improvement over the typical background level of the ^{76}Ge experiments.

For double-β decay in the Majoron channel, the data from 2.0 to 2.63 MeV are studied. There are 95 "two-electron" events in this energy window. Assuming that all the events are due to this channel, we can derive the upper limit of $95+1.3\times\sqrt{95}=108$ for the number of Majoron events at a 90% C.L. Taking into account the efficiencies due to the energy cut, detector containment, and analysis (27%, 33%, and 76%, respectively), we obtain

$$T^{0\nu\chi}_{1/2}>4.9\times10^{21}\text{ yr .}$$

Adopting the matrix elements from the Caltech group [27], this result gives rise to a limit for the effective Majoron-neutrino coupling parameter of

$$\langle g_M\rangle<2.4\times10^{-4}$$

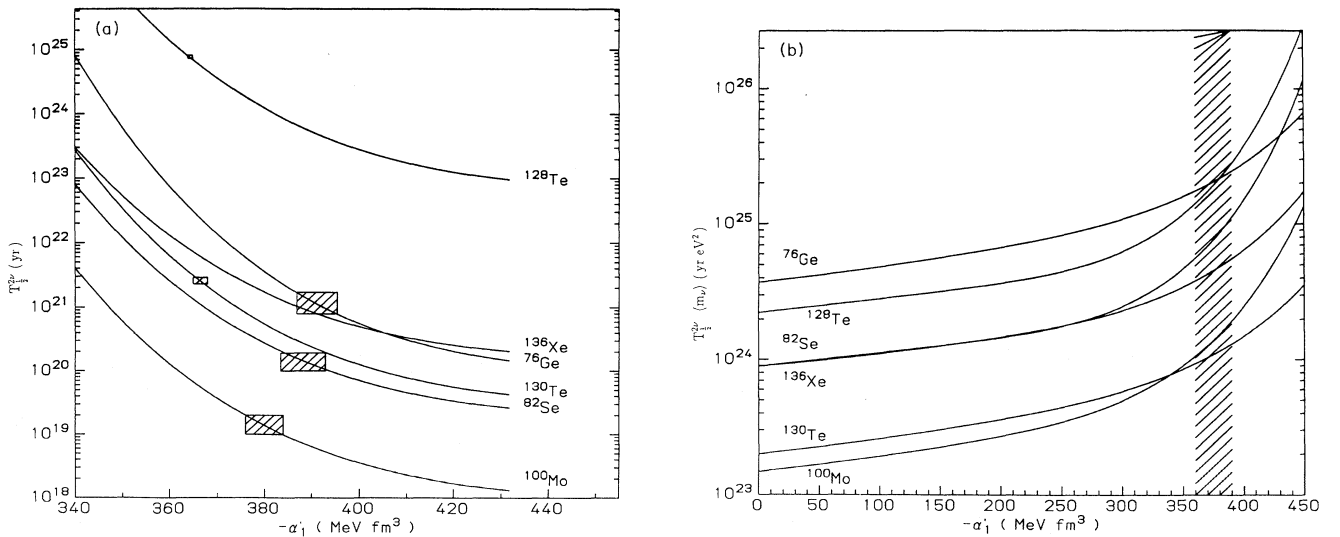FIG. 10. Predictions on (a) $T^{2\nu}_{1/2}$ and (b) $T^{0\nu}_{1/2}\langle m_\nu\rangle^2$ from the Caltech calculations based on a quasiparticle random-phase approximation [27]. The boxes in (a) are experimentally determined 2ν half-lives, while the shaded area in (b) is the range implied by these measurements.

at a 90% C.L. If the geochemical measurement on ^{128}Te is interpreted to be equivalent to a $T_{1/2}^{0\nu\chi}$ limit, the coupling parameter will be $\langle g_M \rangle < 0.2 \times 10^{-4}$. The ^{76}Ge experiment gives a limit of $\langle g_M \rangle < 2.8 \times 10^{-4}$ [30]. These measured limits are to be compared to an estimate of $\langle g_M \rangle \sim 3 \times 10^{-4}$ implied from recent results by the Irvine TPC [8] if the excess of all the high-energy counts is interpreted as due to Majoron emission. For comparison, limits derived from the other calculations are shown in Table II.

The two-electron spectrum can also be used to derive a limit on the 2ν channel. Assuming that all the 246 counts between 1.67 and 2.0 MeV are from $2\nu\beta\beta$, we derive an upper limit of $246 + 1.3 \times \sqrt{246} = 266$ counts due to this channel in this energy window. The respective efficiencies due to energy cuts, detector containment, and analysis are 2.3%, 40%, and 76%. We therefore obtain

$$T_{1/2}^{2\nu} > 2.1 \times 10^{20} \text{ yr}$$

at a 90% C.L., the best limit obtained so far for the 2ν channel in ^{136}Xe. This limit is about a factor of 4–20 below the values predicted by the Caltech [27] and Heidelberg [28] calculations. Comparison with the Caltech predictions is shown in Fig. 10(a).

VI. OUTLOOK

Data taking continues for this experiment in the Gotthard Underground Laboratory. Plans have been drawn up to further reduce the radioactive background level. Boron-loaded polyethylene will be installed around the lead shielding to attenuate the thermal neutron background. Low-background resistors will be used to re-place the existing ones between the field-shaping rings. A cold trap will be constructed to remove the radon contaminants in the xenon. A scintillator system will be set up to veto events related to any surviving cosmic-ray muons. Ultimately, we expect to reach a 0ν sensitivity of better than 10^{24} yr.

In the meantime, further data analysis to study the $2\nu\beta\beta$ and $0\nu\chi$ channels will be pursued. To enhance the sensitivity to the 2ν channel, data will be taken at a lower pressure, where the background rejection for single electrons at the 1-MeV range is optimized. The possibility of performing a difference experiment with xenon depleted in ^{136}Xe will also be investigated.

Excellent tracking performance has been achieved for low-energy (MeV range) completely stopped electrons in the high-pressure xenon TPC. Also demonstrated is the technique of measuring the directionality of low-energy electrons by the difference in dE/dx between their beginnings and ends. This can be a great asset to other experiments at nuclear energies. Based mainly on this work, there is a proposal [31] to measure the neutrino magnetic moment by studying $\bar{\nu}_e$-e scattering of reactor neutrinos at hundreds of keV, using a very similar TPC with CF_4 as the fill gas. Background rejection can be achieved by correlating the scattering angle with the energy of the electrons.

ACKNOWLEDGMENTS

[1] F. Boehm and P. Vogel, *Physics of Massive Neutrinos*, 2nd ed. (Cambridge University Press, Cambridge, England, 1992).

[2] For a recent review on nuclear matrix-element calculations, see T. Tomoda, Rep. Prog. Phys. **54**, 53 (1991).

[3] For a recent review on various double-β decay experiments, see M. K. Moe, Int. J. of Mod. Phys. E (to be published).

[4] T. Kirsten, in *Nuclear Beta Decay and Neutrinos*, Proceedings of the International Symposium, Osaka, Japan, 1986, edited by T. Kotani, H. Ejiri, and E. Takasugi (World Scientific, Singapore, 1986); J. T. Lee et al., Nucl. Phys. **A529**, 29 (1991); A. L. Turkevich et al., Phys. Rev. Lett. **67**, 3211 (1991); T. Bernatowicz et al., ibid. **69**, 2341 (1992).

[5] S. R. Elliott, A. A. Hahn, and M. K. Moe, Phys. Rev. Lett. **59**, 2020 (1987); H. Ejiri et al., Phys. Lett. B **258**, 17 (1991); F. T. Avignone III et al., ibid. **256**, 559 (1991).

[6] For the best published limit on ^{76}Ge, see A. Balysh et al., Phys. Lett. B **283**, 32 (1992).

[7] Y. Chikashige, R. Mohapatra, and R. Reccei, Phys. Lett. **98B**, 265 (1981); G. Gelmini and M. Rondacelli, Phys. Lett. **99B**, 411 (1981); H. M. Georgi, S. L. Glashow, and S. Nussinov, Nucl. Phys. **B193**, 297 (1981).

[8] M. K. Moe, in *Neutrino '92*, Proceedings of the 15th International Conference on Neutrino Physics and Astrophysics, Granada, Spain, 1992, edited by A. Morales (North-Holland, Amsterdam, in press); M. K. Moe et al., UC Irvine Report No. UCI-NEUTRINO 92-1, 1992 (unpublished).

[9] Monsanto Research Corporation, Mound, Oak Ridge (supplier).

[10] G. E. De'Munari and G. Mambriani, Nuovo Cimento A **33**, 299 (1976).

[11] A. S. Barabash et al., Phys. Lett. B **223**, 273 (1989).

[12] E. Bellotti et al., Phys. Lett. B **266**, 193 (1991).

[13] See, for example, T. A. Girard, E. Aprile, and R. C. Fernholz, Nucl. Instrum. Methods A **316**, 44 (1992).

[14] For an overview of the subject, see *The Time Projection Chamber (TRIUMF, Vancouver, 1983),* edited by J. A. Macdonald, AIP Conf. Proc. No. 108 (AIP, New York, 1984).

[15] H. T. Wong, Ph.D. thesis, Caltech, 1991.

[16] D. R. Nygren, Report No. PEP-198, 1975 (unpublished).

[17] H. T. Wong *et al.*, Phys. Rev. Lett. **67**, 1218 (1991).

[18] M. Z. Iqbal *et al.*, Nucl. Instrum. Methods A **259**, 459 (1987).

[19] M. Z. Iqbal, B. M. O'Callaghan, and H. T. Wong, Nucl. Instrum. Methods A **263**, 387 (1988).

[20] J. Thomas *et al.*, IEEE Trans. Nucl. Sci. **NS-34**, 845 (1987).

[21] M. Z. Iqbal *et al.*, Nucl. Instrum. Methods A **243**, 459 (1986).

[22] R. Brun *et al.*, computer code GEANT, version 3.15, CERN, 1992.

[23] M. Doi, T. Kotani, and E. Takasugi, Prog. Theor. Phys. Suppl. **83**, (1985).

[24] Gas-handling components: getter, Matheson hydrox purifier model 8301; circulation pump, Nitto air compressor AC 0102.

[25] Low-background materials: Araldite, resin AY103 and hardener HY951, CIBA-Geigy; circuit board, Rexolite 1422, Oak Materials Group Inc.; insulator, Delrin, the Dupont trade name of a standard acetal.

[26] H. T. Wong *et al.*, Nucl. Instrum. Methods A **329**, 163 (1993).

[27] J. Engel, P. Vogel, and M. R. Zirnbauer, Phys. Rev. C **37**, 731 (1988).

[28] K. Muto, E. Bender, and H. V. Klapor, Z. Phys. A **334**, 177 (1989); **334**, 187 (1989).

[29] J. Suhonen, S. B. Khadkikar, and A. Faessler, Nucl. Phys. **A535**, 91 (1991).

[30] M. Beck *et al.*, Phys. Rev. Lett. **70**, 2853 (1993).

[31] C. Broggini *et al.*, Nucl. Instrum. Methods. A **311**, 319 (1992).